

Available online at website: https://journal.bcrec.id/index.php/bcrec

Bulletin of Chemical Reaction Engineering & Catalysis, 19 (4) 2024, 609-621



Research Article

Conjugated Polyvinyl Alcohol Modified SnO₂ for Efficient Visible Light Photocatalytic Reduction of Cr(VI)

Shaojie Chen^{1,§}, Yuanyuan Luo^{1,2,§}, Yuhan Xu¹, Ying Chen¹, Yinxing Jiang¹, Zhao Li¹, Lin Tian¹, Furong Wang¹, Yuanyuan Liu¹, Jing Li^{1,*}

¹School of Chemistry and Chemical Engineering, Xuzhou University of Technology, Xuzhou, Jiangsu, 221018 China ²School of Chemistry and Chemical Engineering, Yili Normal University, Yining, Xinjiang, 835000, China

Received: 3rd October 2024; Revised: 16th November 2024; Accepted: 16th November 2024 Available online: 23th November 2024; Published regularly: December 2024



Abstract

The photocatalytic activity of tin dioxide (SnO₂) is limited due to its inadequate response to the solar spectrum, wide band gap, and low visible light photocatalytic activity. Here, we synthesized conjugated polyvinyl alcohol (CPVA) modified tin dioxide (CPVA/SnO₂) through in-situ hydrothermal synthesis and evaluated its performance for photocatalytic reduction of hexavalent chromium Cr(VI). A series of testing and characterization results revealed that CPVA was uniformly coated on the surface of SnO₂, forming a mesoporous CPVA/SnO₂ heterojunction with enhanced crystallinity and reduced oxygen defects, which resulted in an expanded light absorption range towards the red light region. The reaction rate constant of CPVA/SnO₂-A for photocatalytic reduction of Cr(VI) under visible light (0.060 min⁻¹) was 6 times higher than that of homemade CPVA/TiO₂ and 2.87 times higher than that of SnO₂ for the photocatalytic reduction of Cr(VI) under UV light (0.0209 min⁻¹). The photocatalytic mechanism indicates that CPVA/SnO₂ exhibited significantly enhanced performance under UV-light irradiation by forming a type II heterojunction. When CPVA/SnO₂ was exposed to visible light, photogenerated electrons on the lowest unoccupied molecular orbital (LUMO) of CPVA were efficiently transferred to the surface of SnO₂ through the CPVA/SnO₂ heterojunction, reducing electron-hole recombination while also photosensitizing the photocatalyst and promoting efficient photocatalysis under visible light illumination. Ultimately, this process effectively reduces Cr(VI) to Cr(III).

Copyright © 2024 by Authors, Published by BCREC Publishing Group. This is an open access article under the CC BY-SA License (https://creativecommons.org/licenses/by-sa/4.0).

Keywords: Polyvinyl Alcohol; CPVA/SnO₂; Heterojunction; Photocatalytic Reduction; Aqueous Cr(VI)

How to Cite: Chen, S., Luo, Y., Xu, Y., Chen, Y., Jiang, Y., Li, Z., Tian, L., Wang, F., Liu, Y., Li, J. (2024). Conjugated Polyvinyl Alcohol Modified SnO₂ for Efficient Visible Light Photocatalytic Reduction of Cr(VI). Bulletin of Chemical Reaction Engineering & Catalysis, 19 (4), 609-621 (doi: 10.9767/bcrec.20226)

Permalink/DOI: https://doi.org/10.9767/bcrec.20226

Supporting Information (SI): https://journal.bcrec.id/index.php/bcrec/article/downloadSuppFile/20226/5313

1. Introduction

As modern industry rapidly advances, environmental and ecological concerns have gained significant prominence. Hexavalent chromium (Cr(VI)), a heavy metal ion primarily originating from the mining, leather production, and dyeing sectors, is of particular concern. Notably, Cr(VI) exhibits high toxicity and mobility in aquatic environments, posing a substantial

threat to the survival of flora and fauna [1-8]. Consequently, there is an urgent global research priority to pursue economical, low-consumption, and effective methods for treating wastewater containing Cr(VI). Photocatalytic technology is known for its cost-effectiveness, high chemical stability and activity, and lack of secondary pollution. Remarkable progress has been made in utilizing photocatalysis to reduce of Cr(VI) in water [7-13].

The photocatalytic reduction of Cr(VI) to less toxic Cr(III) can be effectively achieved by semiconductor photocatalysts, including TiO_2 ,

Email: ljshan@xzit.edu.cn, lijingxz111@163.com (Jing Li)

§ These authors contributed equally.

^{*} Corresponding Author.

 $BC/ZnFe_2O_4$, MoS_2 , SnO_2 , SnS_2 , $g-C_3N_4$, $ZnFe_2O_4$, WO_3/In_2S_3 [2,7,8,11-13]. Among these materials, SnO2 is as a notable metal oxide due to its favorable photogenerated carrier mobility and high UV photocatalytic activity. Additionally, SnO₂ exhibits excellent chemical stability and corrosion resistance while being cost-effective. However, the relatively wide band gap ($E_{\rm g} \sim 3.6$ eV) of SnO₂ limits its solar energy utilization efficiency since it can only be activated by ultraviolet light for photocatalytic reactions [14-Composite heterostructures heterogeneous interfaces have been constructed to enhance the separation of photogenerated electron-hole pairs and improve charge transfer in SnO₂-based systems. For example, Huang [15] constructed a direct Z-scheme SnO₂/Bi₂Sn₂O₇ heterostructure that facilitated charge separation and significantly enhanced the photocatalytic degradation of tetracycline. Wang [16] prepared an efficient SnO₂/TiO₂ heterostructure with abundant oxygen vacancies via in-situ synthesis to achieve efficient charge transfer along with outstanding performance in photocatalytic hydrogen evolution. However, forming extensive and tightly bonded heterojunction contacts is challenging for inorganic metal oxides (M₂O_X). Moreover, factors such as a broad energy band gap and difficulties in structural control have practical the constrained application photocatalytic technology [13]. Conjugated polymers exhibit robust electron supply and carrier transport capabilities, characterized by their HOMO and LUMO energy levels, as well as π-electron conjugated systems linked by C=C and C=N bonds [18]. By leveraging these advantages, modified wide bandgap photocatalysts can enhance the visible light response range [13, 18-21] while facilitating the formation of compact heterojunction interfaces. This effectively promotes interfacial charge transfer, increases charge transport efficiency, and improves the separation of photogenerated electrons and holes.

The study focused on synthesizing CPVA/SnO₂ heterojunctions with conjugated structures using cost-effective water-soluble polyvinyl alcohol (PVA) through in situ hydrothermal synthesis. The synthesized products were characterized to determine their structures and compositions. Furthermore, their performance in photocatalytic Cr(VI) reduction under both visible and ultraviolet light was thoroughly investigated. The mechanisms underlying the enhanced visible light activity of CPVA/SnO₂ heterojunctions were analyzed. The energy band relationships along with electrochemical test results for CPVA/SnO2 was also conducted.

2. Materials and Method

2.1 Chemical Reagents

The specifications of the experimental chemical reagents are comprehensively outlined in Supporting Information Section S1.

2.2 Preparation of Materials

2.1.1 Synthesis of CPVA/SnO₂ heterojunction

A typical synthesis procedure is outlined. To synthesize SnO₂, 5 mmol of SnCl₄·5H₂O and 75 mg of polyvinyl alcohol (PVA) were dissolved in 40 mL of deionized water. The mass ratio of PVA to SnO₂ was maintained at 1:10. The mixture was magnetically stirred for 20 min. Subsequently, the resulting reaction solution was sealed in a stainless steel autoclave and heated in a constant temperature blast dryer oven at 160 °C for 10 h. The precipitate was then washed several times with deionized water and dried in a vacuum oven at 100 °C for 4 h. Finally, the resultant white powder obtained from this process was designated as CPVA/SnO₂-A. This study aims to evaluate the impact of reheat treatment on catalyst properties. CPVA/SnO₂-A was further heated at 180 °C for 2 h to yield CPVA/SnO₂-B.

2.1.2 Synthesis of SnO₂ and CPVA

Furthermore, it should be noted that the white powder form of SnO₂ can also be synthesized separately without incorporating the PVA reagent in the experimental protocol for preparing CPVA/SnO₂. In the experimental scheme for preparing CPVA/SnO₂-A, polyvinyl alcohol (PVA) is utilized as the sole raw material, enabling direct synthesis of CPVA.

2.1.3 Synthesis of CPVA/P25 TiO₂

The synthesis process is as follows: 750 mg of $P25 \text{ TiO}_2$ was dispersed in 40 mL of deionized water, followed by addition of 75 mg of PVA and magnetic stirring until a uniform solution was formed. The mixture was then sealed in a stainless steel autoclave at $160 \,^{\circ}\text{C}$ for $10 \, \text{h}$.

2.1.4 In-situ synthesis of CPVA/TiO₂

Synthetic schemel: 75 mg of PVA was dispersed in 36.8 mL of deionized water, followed by the addition of 3.2 mL of tetrabutyl titanate (TBT). The resulting mixture was stirred to achieve homogeneity before being sealed in a stainless steel autoclave and reacted at 160 °C for 10 h. After completion of the reaction, the precipitate was washed with deionized water, dried in a vacuum oven at 100 °C for 4 h, and grinding into white CPVA/TiO₂ powder.

2.3 Evaluation of Photocatalytic Performance of CPVA/SnO₂ Heterojunction

The photocatalytic activity of the CPVA/SnO₂ heterojunction was evaluated using a 50 mg.L-1 aqueous Cr(VI) as a simulated probe. The experiment was conducted at 25 °C, along with 1 mL of 100 mg.mL⁻¹ citric acid (HCA) solution serving as a hole scavenger, and using 1 g.L-1 CPVA/SnO₂ as the photocatalyst dosage on the heterojunction's CPVA/SnO₂ photocatalytic activity was assessed. The mixed suspension was stirred for 60 min before irradiation to achieve adsorption-desorption equilibrium. A xenon lamp with two filters to block UV light below $\lambda < 420 \text{ nm}$ served as the visible light source, while a highpressure mercury lamp provided the UV light for the CPVA/SnO₂ photocatalytic reduction Cr(VI). After mixing, 4 mL of the reaction mixture was extracted and filtered, followed by measuring the concentration of Cr(VI) in the filtrate using a **UV-Vis** spectrophotometer. The rate photoreduction (Dt) for Cr(VI) was calculated according to Equation (1), where A_t and A_0 represent absorbance values at time t and 0 min, respectively, while c_t and c_0 denote corresponding concentrations of Cr(VI) [8,22].

$$D_t = \left(1 - \frac{A_t}{A_0}\right) \times 100\% = \left(1 - \frac{c_t}{c_0}\right) \times 100\% \tag{1}$$

2.4 Instrumentation for Characterization

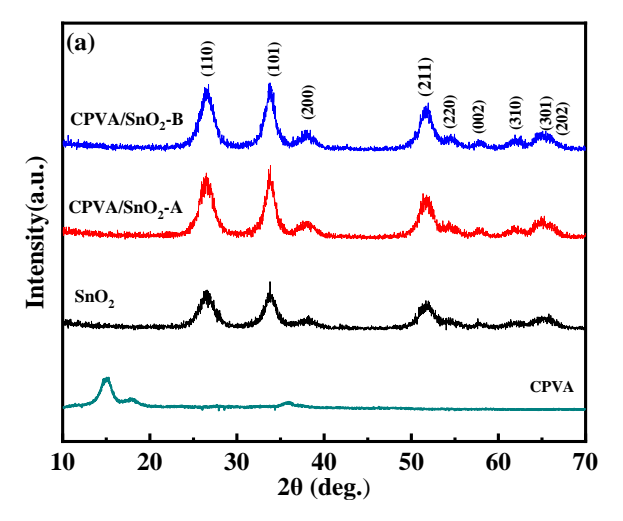
The materials were characterized using various instruments. These included an X-ray Diffractometer (XRD) with Cu- K_a radiation (λ = 0.15406 nm, 40 kV, 200 mA, scanning range of 2θ = 10 ~ 70°). Fourier Transform Infrared Spectrometer (FT-IR) was used with a KBr pellet, and the range of 400 to 4000 cm⁻¹ range was scanned. The Hitachi SU8600 Scanning Electron Microscope (SEM) operating at an acceleration voltage of 15 kV, FEI Tecnai G² F30 S-TWIN field emission High-Resolution Transmission Electron

Microscope (HR-TEM) functioned at 300 kV. A physisorption analyzer was utilized for BET and N₂ adsorption-desorption isotherms analysis. UVvis-Near Infrared Spectrophotometer calibrated with BaSO₄ as a standard reference and covered a scan range from 200 to 800 nm. An Photoelectron Spectrometer employed Al- K_a radiation as the excitation source and was calibrated using C1s at 284.8 eV. The CHI-660D electrochemical workstation photoelectric measured current under illumination from a 23 W LED lamp in 0.1 mol.L-1 Na₂SO₄ solution.

3. Results and Discussion

3.1 Characterization of the As-prepared Photocatalysts

The crystal structure characteristics of the synthesized materials were analyzed using XRD and FTIR. Figure 1(a) presents the XRD patterns of SnO2, CPVA/SnO2, and CPVA. The overall diffraction peaks of the synthesized SnO₂ correspond to tetragonal phase SnO2 (JCPDS card no. 70-4177), with specific peaks observed at 26.58°, 33.81°, 38.04°, and 51.76° correspond to the (110), (101), (200), and (211) crystal planes respectively without any impurity peaks detected indicating successful synthesis of high-purity SnO_2 . CPVA exhibits characteristic two diffraction peaks at 15.06° and 17.96°, while both CPVA/SnO₂-A and CPVA/SnO₂-B displayed similar diffraction patterns, differing only in peak intensity. The CPVA/SnO₂ heterojunction displayed only the characteristic peaks associated with tetragonal phase SnO2 due to the low content of CPVA, resulting in a relatively weak intensity of the diffraction peaks within the composites. Furthermore, it indicates that PVA addition does not significantly affect the crystal structure of SnO₂. Additionally, it was noted that the intensity of the diffraction peaks for the CPVA/SnO₂ heterojunction is more significant than that for



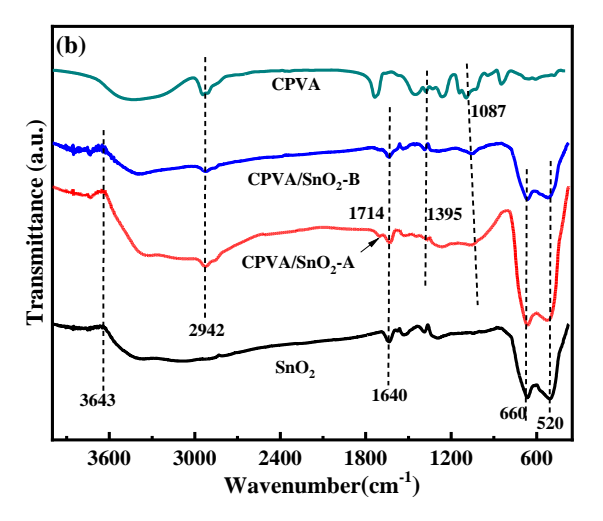


Figure 1. (a) XRD patterns and (b) FT-IR spectra of SnO₂, CPVA, CPVA/SnO₂-A and CPVA/SnO₂-B.

pure SnO₂, implying an enhancement in crystallinity attributed to PVA incorporation. As PVA is a polymer, when combined with SnO₂, its molecular chain can serve as nucleation sites for SnO₂ crystallization, facilitating and enhancing the formation of SnO₂ crystals while improving their degree of crystallinity. Additionally, this process helps inhibit the occurrence of oxygen vacancies [10,23]. The grain sizes calculated for SnO₂, CPVA/SnO₂-A, and CPVA/SnO₂-B are approximately 9 nm, 10 nm, and 11 nm, respectively, determined using Debye-Scherrer formula [20,24], indicating an increase in grain size following reheat treatment [25].

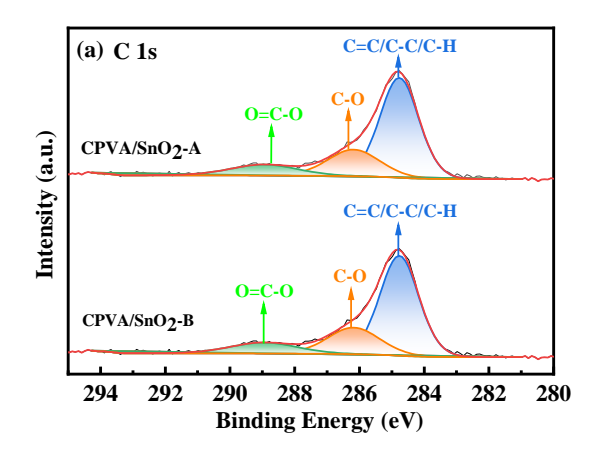
The FT-IR spectra of the synthesized CPVA/SnO₂ heterojunctions are presented in Figure 1(b). The sharp peaks observed at 660 cm⁻¹ and 520 cm⁻¹ corresponded to the asymmetric stretching vibrations of O-Sn-O and symmetric stretching vibrations of Sn-O, respectively [19,26,27]. Characteristic absorption peaks at 2942, 1714, 1640, 1395, and 1087 cm⁻¹ were attributed to the vibrations of C-H, C=C, C=O, C-C, and C-OH bonds [12,21,28]. The presence of the C=C bond indicated that a conjugated structure was formed through a hydrothermal reaction between CPVA and SnO₂. Meanwhile, the C=O groups suggested dehydration of PVA during heat treatment. The absorption peak at $3640~\mathrm{cm^{-1}}$ for all samples was associated with the stretching vibrations of O-H from water adsorbed on the sample surface. Compared to the infrared spectra of CPVA and SnO2, the characteristic peaks at 2949 and 1087 cm⁻¹ in CPVA/SnO₂-A exhibited slight shifts, indicating that strong interaction exists between CPVA and SnO2 [29,30]. This suggested that the CPVA/SnO₂ stable possessed a interface heterojunction.

The surface chemical composition and valence state of the CPVA/SnO₂ heterojunction were analyzed using XPS. High-resolution spectra of C1s and O1s in CPVA/SnO₂-A and CPVA/SnO₂-B were presented in Figure 2. The C1s high-

resolution spectrum revealed three distinct peaks at 284.80, 286.09, and 288.77 eV. The peak at 284.80 eV is attributed to C-C, C=C, or C-H bonds, while the 286.09 and 288.77 eV corresponded to C-O and O=C-O [19,31]. The high-resolution spectra for O1s in both CPVA/SnO₂-A and CPVA/SnO₂-B exhibited three peaks at 531.18 eV, 532.58 eV, and 533.07 eV, which corresponded to lattice oxygen in SnO₂ as well as C-O, and C=O, respectively [20,21,26]. The XPS peak separation software calculated the O1s spectrum of CPVA/SnO₂-A, revealing that the peak areas for C-O and O=C-O bonds were determined to be 41.42% and 7.24%, respectively. Similarly, in CPVA/SnO₂-B, the corresponding peak areas for C-O and O=C-O bonds were 30.61% 3.32%, and respectively. experimental results may be due to the presence of oxygen defects in the photocatalyst. The results of XPS analysis further confirmed the existence of CPVA in the synthesized composites [29,32].

The samples were morphologically characterized using SEM and HRTEM, as illustrated in Figure 3. SnO₂ (Figure 3a), CPVA/SnO₂-A (Figure 3b), and CPVA/SnO₂-B (Figure 3c) primarily consisted of aggregated nanoparticles. Notably, a noticeable sintering phenomenon was observed in the case of CPVA/SnO₂-B. The HR-TEM image CPVA/SnO₂-A presented in Figure 3(d) not only revealed distinct lattice fringes characteristic of tetragonal phase SnO₂ but also displayed nearly amorphous regions of CPVA on the surface and edges of the SnO₂ nanocrystals, forming a closely contacted heterojunction that facilitates transfer pathway for photogenerated electrons from CPVA to SnO₂ under visible light irradiation.

The EDX spectra and elemental mapping images of CPVA/SnO₂-A are provided in Figure 3(e)~(i), demonstrating a uniform distribution of Sn, O, and C elements throughout the sample, further confirming the composition of the photocatalysts. Figures S2 and S3 in the Supporting Information (SI) showed the EDX



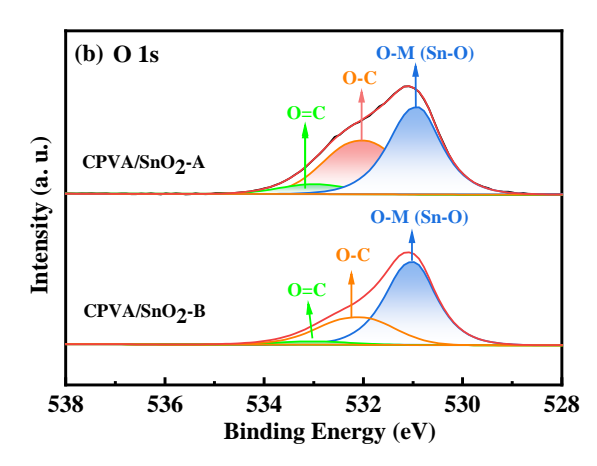


Figure 2. High-resolution spectra of XPS: (a) C1s, (b) O1s of CPVA/SnO₂-A and CPVA/SnO₂-B.

elemental mapping images for both SnO2 and CPVA/SnO₂-B, and Table S1 listed the elemental content across various samples. These results confirmed that the atomic ratio of Sn to O in both CPVA/SnO₂-A (1:2.32) and CPVA/SnO₂-B (1:2.55) exceeded that found in pure SnO_2 (1:1.75), indicating an enhancement in crystallinity due to PVA modification alongside a reduction in oxygen defects within the CPVA/SnO₂. The possible reasons for this result are that the interaction between CPVA and SnO2 alters the electronic structure of the SnO₂ crystal [29,32,33], thereby impeding the formation of oxygen vacancies. Moreover, CPVA contains oxygen, which serves as an oxygen source during the formation process of CPVA/SnO₂-A, leading to a reduction in oxygen vacancies within the SnO₂ crystal. This reduction in oxygen defects is advantageous for enhancing photogenerated carrier utilization and potentially improving photocatalytic performance.

3.2 Photocatalytic Performance

The absorption response of PVA in the visible light region is not observed, as shown in Figure 4(a). However, CPVA demonstrated a distinct

absorption signal within 300 to 800 nm after hydrothermal treatment. This indicated the transformation of PVA into CPVA with C=C conjugated double bonds. Additionally, SnO₂, CPVA/SnO2-A, and CPVA/SnO2-B all displayed similar UV absorption spectra (λ < 400 nm). In contrast, SnO_2 nanoparticles showed significant light absorption signal within the visible light range from 400 to 700 nm. However, due to its C=C conjugated structure, CPVA/SnO₂ exhibited enhanced visible light absorption. Consequently, CPVA/SnO₂ demonstrates photocatalytic activity under visible light irradiation. Based on Tauc plots presented in Figure 4(b), the estimated bandgap values for SnO₂, CPVA/SnO₂-A, CPVA/SnO₂-B, and CPVA are found to be 3.40 eV, 2.52 eV, 2.91 eV, and 2.45 eV, respectively. Incorporating CPVA into the SnO₂ band structure introduces new energy thereby reducing $_{
m the}$ band Furthermore, due to varying degrees of oxygen defects in CPVA/SnO₂-A and CPVA/SnO₂-B, there are changes in electronic band structure, which result in increased energy required for electron transition in CPVA/SnO₂-B and a higher band gap

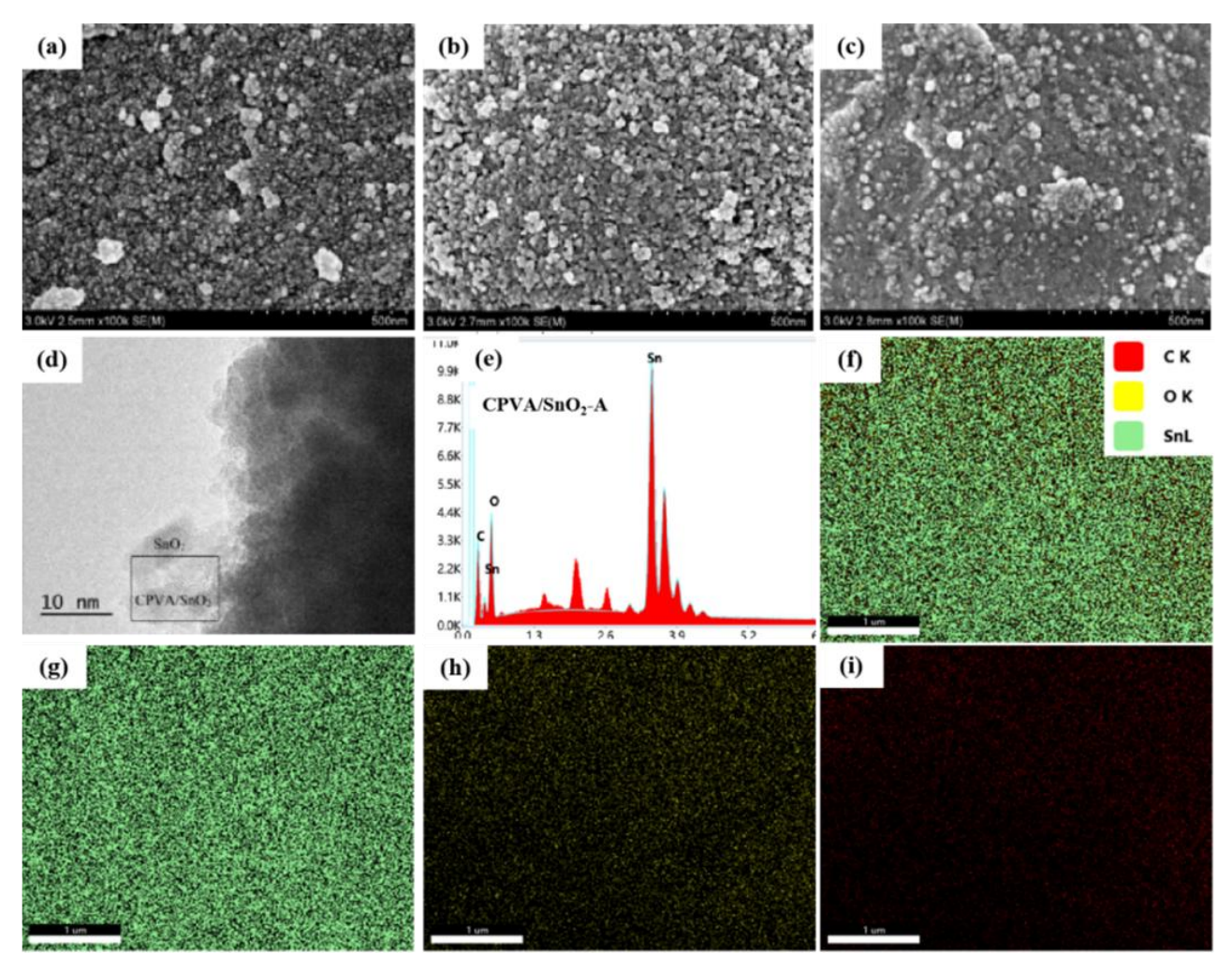


Figure 3. SEM images of (a) SnO₂, (b) CPVA/SnO₂-A and (c) CPVA/SnO₂-B, (d) HR-TEM image of CPVA/SnO₂-A, (e) EDX spectrum of CPVA/SnO₂-A, and elemental mapping images of (f) CPVA/SnO₂-A, (g) Sn, (h) O and (i) C.

energy than that observed in CPVA/SnO₂-A [30]. These experimental results confirm that conjugated poly(vinyl alcohol) effectively reduces the bandgap value of SnO₂.

The photocatalytic activity of CPVA/SnO₂ heterojunction modified with conjugated polymer was assessed, and the performance of the synthesized photocatalysts for the photocatalytic reduction of aqueous Cr(VI) was evaluated using UV and visible light as excitation sources, respectively. The semiconductors SnO2, TiO2, and P25 TiO₂ depicted in Figure 5(a) possess wide band gaps that render them ineffective in utilizing visible light to to generate photogenerated electrons and holes efficiently. Consequently, it does not exhibit visible-light-driven photocatalytic reduction of aqueous Cr(VI). In contrast, both CPVA/SnO₂-A and CPVA/SnO₂-B demonstrated enhanced photocatalytic activity under visible light irradiation, with CPVA/SnO₂-A achieving complete (~100%) photocatalytic reduction of Cr(VI) after 120 min of exposure to visible light. enhanced photocatalytic activity CPVA/SnO₂-A compared to CPVA/SnO₂-B can be attributed to the grain growth observed in CPVA/SnO₂-B upon heating, which leads to the disruption of active sites on the photocatalyst surface. Consequently, this alteration affects the surface chemical environment and influences adsorption and electronic transition behaviors [29,30]. As a result, CPVA/SnO₂-B exhibits an increased band gap energy and diminished photocatalytic activity. However, all samples exhibited effective UV-induced photocatalytic reduction of Cr(VI), as shown in Figure 5(b), with visible-light photocatalytic activity CPVA/SnO₂-A surpassing that both CPVA/SnO₂-B and SnO₂.

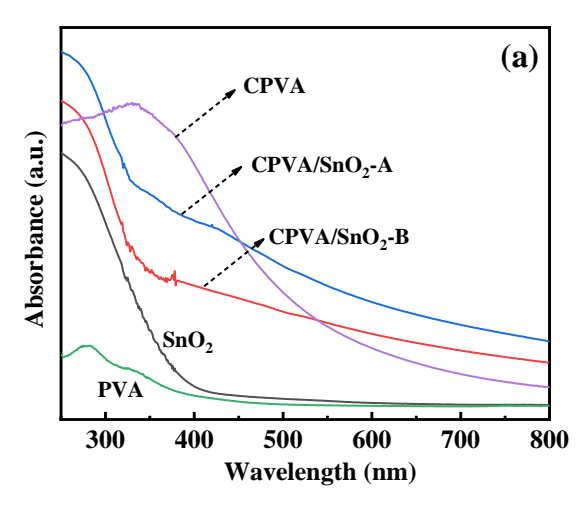
The pseudo-first-order kinetics model (Eq. 2) [34-36] was employed to quantitatively compare the reaction rate constants (k) for the photocatalytic reduction of Cr(VI). Here c_{i0} and c_{it}

denote the concentration of aqueous Cr(VI) at time t and 0 min, respectively.

$$\ln\left(\frac{c_{i0}}{c_{it}}\right) = kt_i \tag{2}$$

By plotting ln (c_{i0}/c_{it}) against t_i , the rate constants (k) along with correlation coefficients (R^2), for the photocatalytic reduction of Cr(VI), were obtained under both UV and visible light irradiation for SnO₂, CPVA/SnO₂-A, and CPVA/SnO₂-B as illustrated in Figures 5(c) and 5(d). The results indicated that CPVA/SnO2-A exhibited a superior photocatalytic reduction of Cr(VI) compared to SnO₂ under visible and UV irradiation. Precisely, during the visible light reaction, the rate constant of CPVA/SnO2 was measured at 0.060 min-1, which is higher than that observed during UV light reaction at 0.0594 min⁻¹, and approximately 2.87 times greater than that associated with UVinduced photocatalytic reduction of Cr(VI) by SnO₂ (0.0209 min⁻¹). Therefore, these findings suggest that CPVA/SnO₂-A is an effective photocatalyst for reducing Cr(VI) under both UV and visible light irradiation.

Titanium oxide (TiO2) is a widely used catalyst due to its high chemical stability, photocatalytic excellent activity, good photochromic properties, non-toxicity, and low [35,37]. This study compared photocatalytic properties of CPVA/TiO2 and CPVA/SnO₂. According to the preparation method and experimental parameters of CPVA/SnO₂, we synthesized CPVA/P25 TiO2 and CPVA/TiO2 using tetrabutyl titanate and P25 TiO2 as the raw materials. As shown in Fig. 5a~c, the Cr (VI) reduction rate by CPVA/P25 TiO2 and CPVA/TiO2 increased continuously with the prolongation of visible and UV irradiation time. photocatalytic activity of CPVA/P25 TiO2 and CPVA/TiO₂ was weaker than that of CPVA/SnO₂, and both CPVA/TiO2 and CPVA/SnO2-A achieved



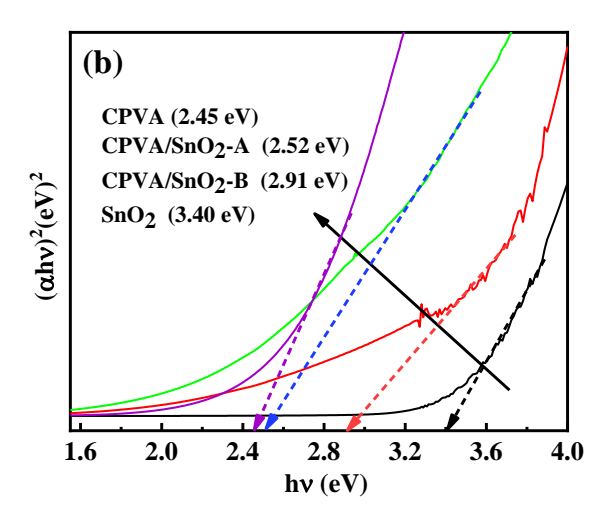


Figure 4. (a) UV-vis diffuse reflection spectra, (b) Tauc plots of SnO₂, CPVA/SnO₂-A, CPVA/SnO₂-B and CPVA.

a 100% reduction of Cr(VI) after 160 min of UV irradiation. After 160 min of visible light irradiation, CPVA/TiO₂ was able to reduce 72.8% of Cr(VI) photocatalytically, and the photocatalytic reaction rate constants of CPVA/SnO₂-A were 3.75 times higher than those of CPVA/P25 TiO₂ and 6 times higher than those of CPVA/TiO₂. This demonstrates that C=C

conjugated double bonds in CPVA significantly enhance its photocatalytic activity when combined with SnO₂.

 N_2 adsorption-desorption isotherms and transient photocurrent response signals were employed to analyze the factors influencing photocatalytic activity. Figure 6(a) illustrates the N_2 adsorption-desorption isotherms for SnO_2 ,

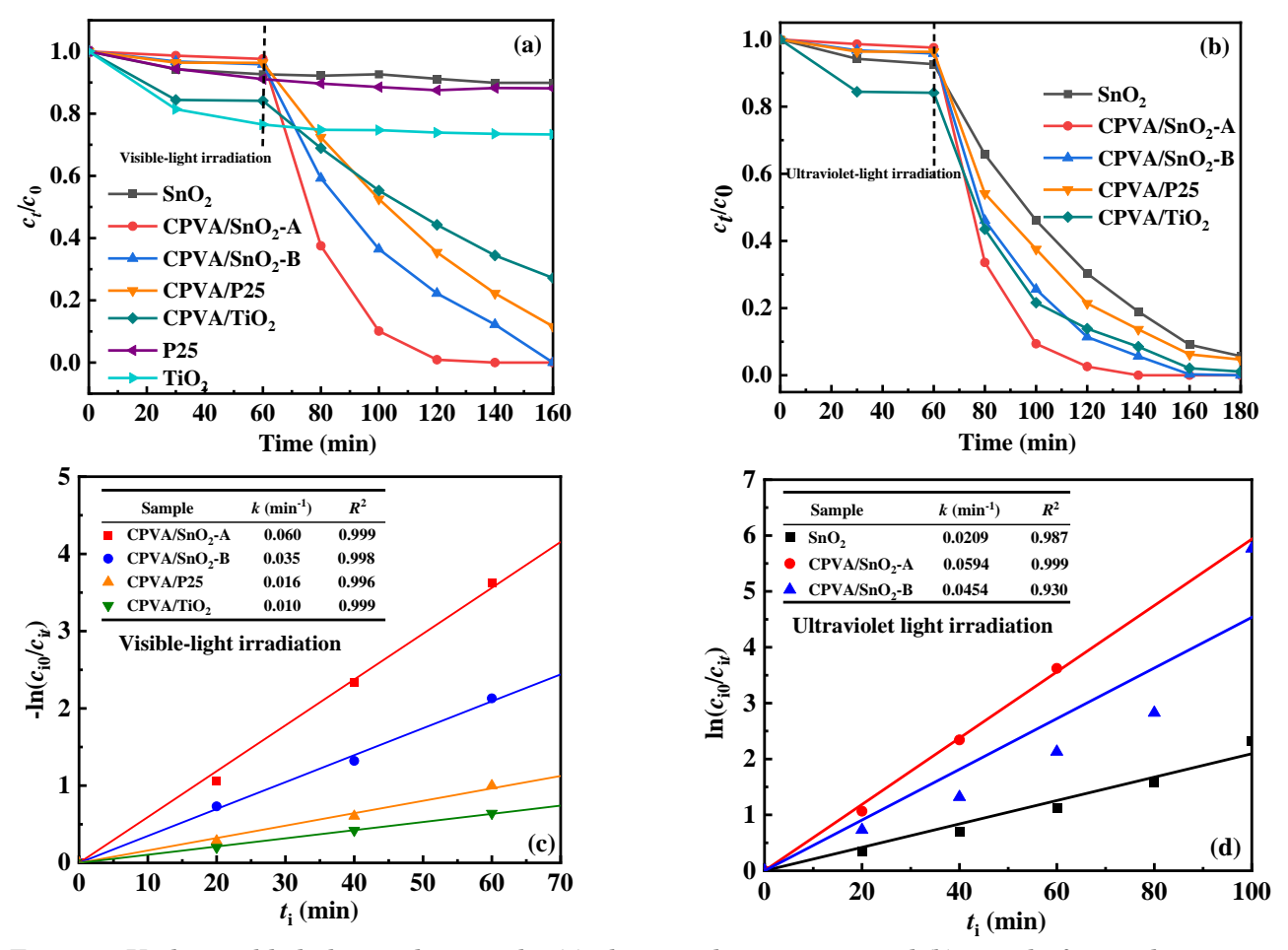


Figure 5. Under visible light irradiation, the (a) photocatalytic activity and (b) pseudo-first-order reaction rate constants for Cr(VI) reduction by SnO₂, CPVA/SnO₂-A, CPVA/SnO₂-B, CPVA/P25 TiO₂, and CPVA/TiO₂ were evaluated; under ultraviolet light drive, the (c) photocatalytic activity and (d) rate constants (*k* values) for SnO₂, CPVA/SnO₂-A, and CPVA/SnO₂-B were assessed using the plots of ln(*cio/cii*) vs. *t*.

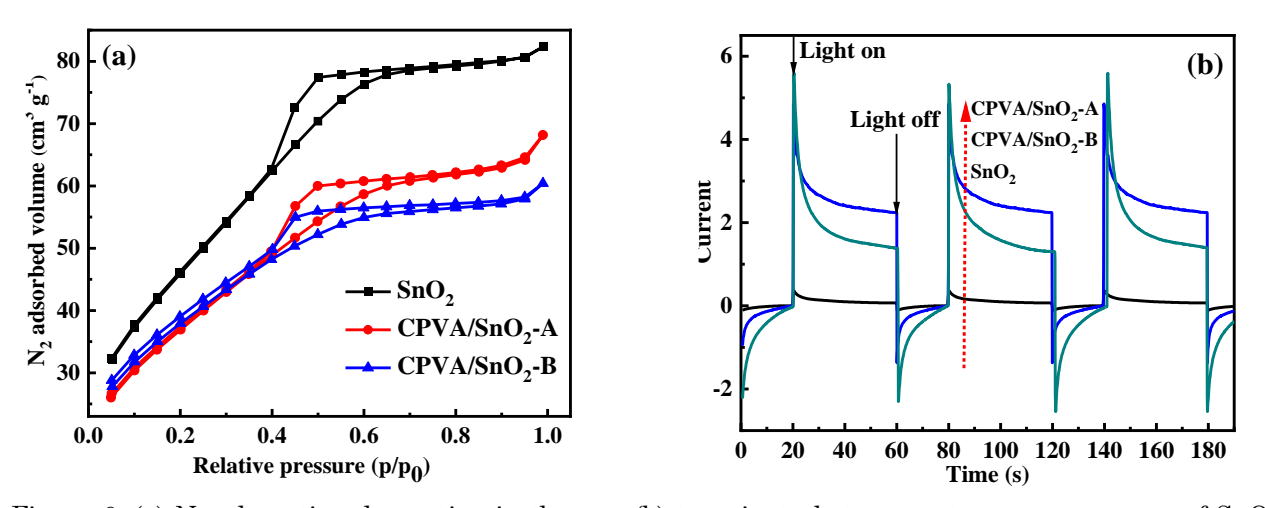


Figure 6. (a) N₂ adsorption-desorption isotherms, (b) transient photocurrent response spectra of SnO₂, CPVA/SnO₂-A and CPVA/SnO₂-B.

CPVA/SnO2-A, and CPVA/SnO2-B. photocatalysts exhibited IV-type isotherms with hysteresis loops in the relative pressure range of 0.4 to 1.0 (p/p_0) , which indicates that all synthesized photocatalysts possess mesoporous structures [19,31]. The specific surface areas of SnO₂, CPVA/SnO₂-A, and CPVA/SnO₂-B were determined to be 170.5, 128.2, and 133.1 m².g⁻¹, respectively, using the Brunauer-Emmett-Teller Photocatalytic (BET) method. experiments further demonstrated that the adsorption capacity of the synthesized photocatalysts for Cr(VI) correlates with their specific surface areas, reflecting that a larger specific surface area of the photocatalysts provides more surface active sites. In addition, the specific surface area is a crucial impacts the performance factor that photocatalysts; however, it is not the sole determinant [29-36]. A larger specific surface area typically implies an increased number of active sites and a greater contact area, thereby enhancing photocatalytic efficiency through improved contact efficiency between the photocatalyst and reactant. The CPVA/SnO₂-A exhibits the most superior photocatalytic effect, which may be influenced by multiple factors including active sites on the catalyst surface, surface defects, light absorption efficiency of the catalyst, and interface structure of the composite material providing a pathway for photogenerated carrier transport. We have provided additional explanations in the document.

The photocurrent of CPVA/SnO₂-A is higher than that of both CPVA/SnO2-B and SnO2, as depicted in Figure 6(b), suggesting the efficient generation and separation of photoinduced electron-hole pairs by CPVA/SnO₂-A. Consequently, it exhibits superior activity for the visible-induced photocatalytic reduction of Cr(VI). The mechanism underlying the photocurrent generation in these prepared photocatalysts can be explained as follows: upon illumination from a light source, the electrons transition from the valence band (VB) of SnO₂ to the conduction band (CB) of SnO₂, while HOMO orbitals of CPVA

transition to the LUMO orbitals, facilitating directional the movement of the electrons.

3.3 Photocatalytic Mechanism Analysis

Based on experimental results and data analysis, we have proposed a mechanism for the photocatalytic reduction of Cr(VI) under visible light in CPVA/SnO₂-A. SnO₂ and CPVA are n-type semiconductors, as illustrated in Figure 7. The conduction band (CB, -0.20 eV) and valence band (VB, 3.20 eV) potentials of SnO₂ are indisputably lower than the energy levels of the lowest unoccupied molecular orbital (LUMO, -0.5 eV), and the highest occupied molecular orbital (HOMO, VB, 1.95 eV) of CPVA. Consequently, SnO₂ and CPVA exhibit a well-matched band structure. CPVA functioning as an electron donor while SnO₂ acts as an electron acceptor.

Under visible light irradiation (Figure 7(a)), SnO_2 , being a wide bandgap semiconductor ($E_g =$ 3.40 eV), is unable to effectively utilize visible light to generate photogenerated electrons and holes. In contrast, CPVA ($E_g = 2.45 \text{ eV}$) can absorb energy from visible light photons to excite electrons (e) from its HOMO orbital to the LUMO orbital while photogenerated holes (h^+) remain in the HOMO orbital. These excited photogenerated electrons subsequently transfer to the conduction band of SnO₂ through the heterojunction interface between CPVA/SnO₂-A. Consequently, adsorbed Cr(VI) on the photocatalyst surface is reduced to Cr(III). This process significantly enhances the efficiency of photocatalytic reduction under visible light.

Figure 7(b) depicts the UV-driven photocatalytic reaction, which shows that both CPVA and SnO_2 absorb energy from UV photons, thereby generating photoinduced electrons and holes. The energy band structure of CPVA and SnO_2 are well-matched, ensuring efficient transfer of photoinduced electrons from the LUMO orbitals of CPVA to the CB of SnO_2 through the composite heterojunction interface. Similarly, photoinduced holes in the VB of SnO_2

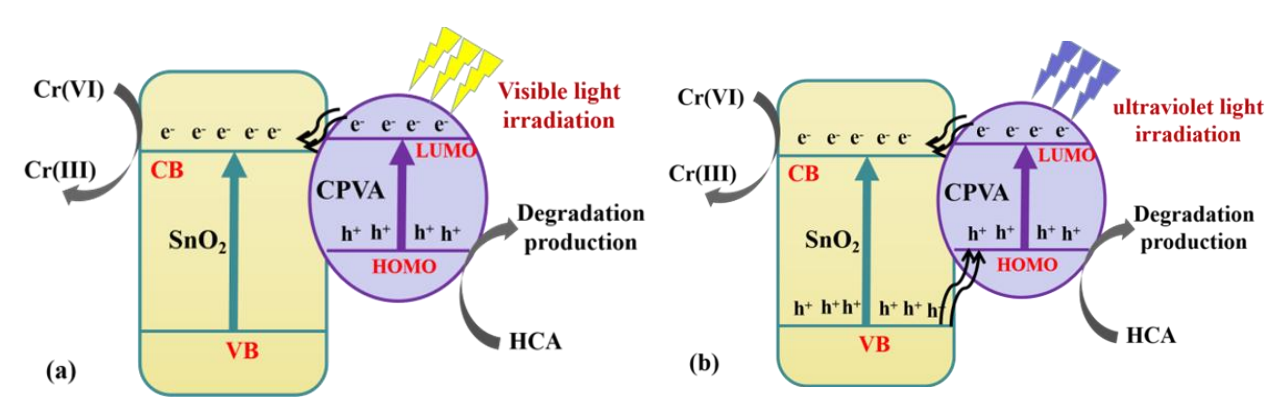


Figure 7. Photocatalytic Cr(VI) reduction mechanism of CPVA/SnO₂-A under (a) visible light, (b) UV light irradiation.

migrate to the HOMO orbitals of CPVA via this heterogeneous interface. This process effectively separates charge carriers within the bulk material. However, the photoinduced carriers remain in energy bands with weaker oxidation and reduction capabilities, limiting their photocatalytic activities.

4. Conclusions

This study fabricated mesoporous CPVA/SnO₂ heterojunctions capable responding to visible light using an in-situ hydrothermal synthesis method. The results clearly show that CPVA can be uniformly deposited on the surface of tin dioxide to form a stable CPVA/SnO₂ heterojunction characterized by increased crystallinity and reduced oxygen defects, while facilitating photogenerated carrier transport. A type II CPVA/SnO₂ heterostructure is formed during UV-driven photocatalytic Cr(VI) The visible-light photocatalytic reduction. reaction shows that photogenerated electrons at the LUMO level of CPVA were transported to the SnO_2 surface through the CPVA/SnO₂ heterojunction. This process sensitizes SnO2 and mitigates the recombination events involving photo-induced electrons and holes within the photocatalyst, enhancing efficiency for visible light-mediated photocatalytic reduction of Cr(VI).

Acknowledgments

We thank for the Science and Technology Project of Xuzhou (NO. KC21286), Jiangsu Provincial Natural Science Foundation (BK20240332), the Natural Natural Science Foundation of China (NO. 22202169), and Innovation and entrepreneurship projects for college students (xcx2024002).

CRediT Authors Statement

Jing Li: Writing – Project administration, original draft, Review & Editing, Funding acquisition. Zhao Li, and Yuanyuan Liu: Supervision, Funding acquisition. Lin Tian, Ying Chen, and Furong Wang: Review & Editing. Shaojie Chen, Yuanyuan Luo, Yuhan Xu, and Yinxing Jiang: Visualization, Investigation. All authors have read and agreed to the published version of the manuscript.

References

- [1] Wang, C.C., Du, X.D., Li, J., Guo, X.X., Wang, P., Zhang, J. (2016). Photocatalytic Cr (VI) reduction in metal-organic frameworks: A minireview. Applied Catalysis B: Environmental, 193, 198-216. DOI: 10.1016/j.apcatb.2016.04.030.
- [2] Liu, Z., Yu, Y., Zhu, X., Fang, J., Xu, W., Hu, X., Li, R., Yao, L., Qin, J., Fang, Z. (2022). Semiconductor heterojunctions for photocatalytic hydrogen production and Cr (VI) Reduction: A review. *Materials Research Bulletin*, 147, 111636. DOI: 10.1016/j.materresbull.2021.111636.
- [3] Li, Q., Zhuang, X., Zhou, G., Yang, Z., Yang, T., Xiao, H., Xu, T., Wang, W. (2023). Efficient removal of Cr(VI) from wastewater by ZnO-polyacrylic acid/cellulose fiber/polyethylene glycol hydrogel: Synergistic effect of adsorption and photocatalytic reduction. *Journal of Environmental Chemical Engineering*, 11(5), 110390. DOI: 10.1016/j.jece.2023.110390.
- [4] Xing, X., Zhang, L., Ren, Y., Li, Y., Yu, H., Shi, W. (2024). Double bismuth-based Bi₂S₃/Bi₂MoO₆ S-scheme heterojunction for ultrafast photocatalytic removal of Cr (VI). Journal of Environmental Chemical Engineering, 12(2), 112122. DOI: 10.1016/j.jece.2024.112122.
- [5] Zhao, F., Liu, Y., Hammouda, S.B., Doshi, B., Guijarro, N., Min, X., Tang, C., Sillanpää, M., Sivula, K., Wang, S. (2020). MIL-101 (Fe)/g-C₃N₄ for enhanced visible-light-driven photocatalysis toward simultaneous reduction of Cr(VI) and oxidation of bisphenol A in aqueous media. Applied Catalysis B: Environmental. 272, 119033. DOI: 10.1016/j.apcatb.2020.119033.
- [6] Zhang, J., Zhang, W., Yuan, F., Yang, Z., Lin, J., Huang, Y., Ding, M. (2021). Effect of Bi₅O₇I/calcined ZnAlBi-LDHs composites on Cr (VI) removal via adsorption and photocatalytic reduction. Applied Surface Science, 562, 150129. DOI: 10.1016/j.apsusc.2021.150129.
- [7] Luo, N., Chen, C., Yang, D., Hu, W., Dong, F. (2021). S defect-rich ultrathin 2D MoS₂: the role of S point-defects and S strip-defects in the removal of Cr (VI) via synergistic adsorption and photocatalysis. *Applied Catalysis B: Environmental*, 299, 120664. DOI: 10.1016/j.apcatb.2021.120664.
- [8] Shen, X., Zheng, T., Yang, J., Shi, Z., Xue, Q., Liu, W., Shan, S., Wong, M. (2020). Removal of Cr (VI) from acid wastewater by BC/ZnFe₂O₄ magnetic nanocomposite via the synergy of absorption-photocatalysis. *ChemCatChem*, 12(16), 4121-4131. DOI: 10.1002/cctc.202000619.
- [9] Long, Z., Zhang, G., Du, H., Zhu, J., Li, J. (2021). Preparation and application of BiOBr-Bi₂S₃ heterojunctions for efficient photocatalytic removal of Cr (VI). Journal of Hazardous Materials, 407, 124394. DOI: 10.1016/j.jhazmat.2020.124394

- [10] Wang, K., Chen, P., Nie, W., Xu, Y., Zhou, Y. (2019). Improved photocatalytic reduction of Cr (VI) by molybdenum disulfide modified with conjugated polyvinyl alcohol. *Chemical Engineering Journal*, 359, 1205-1214. DOI: 10.1016/j.cej.2018.11.057.
- [11] Islam J.B., Furukawa M., Tateishi I., Katsumata, H., Kaneco, S. (2021). Formic acid motivated photocatalytic reduction of Cr (VI) to Cr (III) with ZnFe₂O₄ nanoparticles under UV irradiation. *Environmental Technology*, 42(17), 2740-2748. DOI: 10.1080/09593330.2020.1713902.
- [12] Zhang, M., Liu, X. (2022). Direct Z-scheme WO₃/In₂S₃ heterostructures for enhanced photocatalytic reduction Cr(VI). *Journal of Alloys and Compounds*, 908, 164488. DOI: 10.1016/j.jallcom.2022.164488.
- [13] Zhang, F., Zhang, Y., Zhou, C., Yang, Z., Xue, H., Dionysiou, D.D. (2017). A new high efficiency visible-light photocatalyst made of SnS₂ and conjugated derivative of polyvinyl alcohol and its application to Cr(VI) reduction. *Chemical Engineering Journal*, 324, 140-153. DOI: 10.1016/j.cej.2017.05.009.
- [14] Silva, E., Alvarado-Beltrán, C.G., Gaxiola, A., Orozco-Carmona, V.M., Luque, P.A., Castro-Beltrán, A. (2023). A new green procedure to obtain and photosensitize SnO₂, in one step, for solar photocatalysis using natural dyes. *Ceramics International*, 49(11), 16732-16739. DOI: 10.1016/j.ceramint.2023.02.034.
- [15] Huang, S., Zhang, J., Qin, Y., Song, F., Du, C., Su, Y. (2021). Direct Z-scheme SnO₂/Bi₂Sn₂O₇ photocatalyst for antibiotics removal: Insight on the enhanced photocatalytic performance and promoted charge separation mechanism. Journal of Photochemistry and Photobiology A: Chemistry. 404, 112947. DOI: 10.1016/j.jphotochem.2020.112947.
- [16] Wang, H., Liu, J., Xiao, X., Meng, H., Wu, J., Guo, C., Zheng, M., Wang, X., Guo, S., Jiang, B. (2023). Engineering of SnO₂/TiO₂ heterojunction compact interface with efficient charge transfer pathway for photocatalytic hydrogen evolution. *Chinese Chemical Letters*, 34(1), 107125. DOI: 10.1016/j.cclet.2022.01.018.
- [17] Liang, X., Dai, R., Wang, Q., Zhang, B. (2023). Antibacterial activity of SnO₂ in visible light enhanced by erbium-cobalt co-doping. *Colloids* and Surfaces A: Physicochemical and Engineering Aspects, 676, 132257. DOI: 10.1016/j.colsurfa.2023.132257.
- [18] Ponnamma, D., Elgawady, Y., Nair, S.S., Hassan, M.K., Al-Maadeed, M. (2022). Core-shell nanofibers of polyvinyl alcohol/polylactic acid containing TiO₂ nanotubes for natural sunlight driven photocatalysis. *Macromolecular Materials and Engineering*, 307(2), 2100482. DOI: 10.1002/mame.202100482.

- [19] Zhang, J., Yang, H., Jiang, L., Dan, Y. (2016). Enhanced photo-catalytic activity of the composite of TiO₂ and conjugated derivative of polyvinyl alcohol immobilized on cordierite under visible light irradiation. *Journal of energy chemistry*, 25(1), 55-61. DOI: 10.1016/j.jechem.2015.10.010.
- [20] Li, J., Peng, T., Zhang, Y., Zhou, C., Zhu, A. (2018). Polyaniline modified SnO₂ nanoparticles for efficient photocatalytic reduction of aqueous Cr(VI) under visible light. Separation and Purification Technology, 201, 120-129. DOI: 10.1016/j.seppur.2018.03.010.
- [21] Zhang, L., Qi, H., Zhao, Y., Zhong, L., Zhang, Y., Wang, Y., Xue, J., Li, Y (2019). Au nanoparticle modified three-dimensional network PVA/RGO/TiO₂ composite for enhancing visible light photocatalytic performance. *Applied Surface Science*, 498, 143855. DOI: 10.1016/j.apsusc.2019.143855.
- [22] Wu, X., Chen, S., Jiang, Y., Zhao, X., Li, Z., Zhou, Y., Li, J. (2023). 1D/2D Rod-sheet shape Bi₂S₃ photocatalyst for photocatalytic reduction Cr (VI) under visible light. Bulletin of Chemical Reaction Engineering & Catalysis, 18(4). DOI: 10.9767/bcrec.20054.
- [23] Chen, J., Wang, B., Wang, J., Zhang, Y. (2022). Development of a new high-performance visible-light photocatalyst by modifying tin disulfde with cyclized polyacrylonitrile. *Materials Letters*, 330, 133353. DOI: 10.1016/j.matlet.2022.133353.
- [24] Sasikala, S., Balakrishnan, M., Kumar, M., Chang, J.H. (2023). Effect of solvent mixtures on the unique morphology for photocatalytic activity of Bi₂S₃ nanoparticles synthesized by microwave irradiation method. *Inorganic* Chemistry Communications, 153, 110854. DOI: 10.1016/j.inoche.2023.110854.
- [25] Haider, A., Ali., Cun, Y., Bai, X., Xu, Z., Zi, Y., Qiu, J., Song, Z., Huang, A., Yang, Z. (2022). Anti-counterfeiting applications by photochromism induced modulation of reversible upconversion luminescence in TiO₂:Yb³⁺, Er³⁺ ceramic. *Journal of Materials Chemistry C*, 10, 6243. DOI: 10.1039/d2tc00859a.
- [26] Kandasamy, M., Seetharaman, A., Sivasubramanian, D., Nithva. A., K., Jothivenkatachalam, Maheswari, N., Gopalan, M., Dillibabu, S., Eftekhari, A. (2018). Ni-doped SnO2 nanoparticles for sensing and photocatalysis. ACS Applied Nano Materials, 1(10), 5823-5836. DOI: 10.1021/acsanm.8b01473.
- [27] Kumar, M.R., Murugadoss, G., Venkatesh, N., Sakthivel, P. (2020). Synthesis of Ag₂O-SnO₂ and SnO₂-Ag₂O nanocomposites and investigation on photocatalytic performance under direct sun light. *ChemistrySelect*, 5(23), 6946-6953. DOI: 10.1002/slct.202001227.
- [28] Emami, S., Alavi Nikje, M.M. (2018). Magnetic Fe₃O₄/SiO₂/NH₂ as the recyclable heterogeneous nanocatalyst on bisphenol-A recovery from polycarbonate wastes. *Russian Journal of Applied Chemistry*, 91, 159-166. DOI: 10.1134/s107042721801024x.

- [29] Wang, J., Chen, Y. (2022). Simple synthesis of conjugated polyvinyl alcohol derivative-modified ZnFe₂O₄ nanoparticles with higher photocatalytic efficiency. *Powder Technology*, 402 117360. DOI: 10.1016/j.powtec.2022.117360.
- [30] Premkumar, H. (2024). Synthesis, characterization and photocatalytic performance of polyvinyl alcohol/zinc oxide nanocomposites: A comprehensive study. *Nano-Structures & Nano-Objects*, 39, 101208. DOI: 10.1016/j.nanoso.2024.101208.
- [31] Bardestani, R., Patience, G.S., Kaliaguine, S. (2019). Experimental methods in chemical engineering: specific surface area and pore size distribution measurements-BET, BJH, and DFT. The Canadian Journal of Chemical Engineering, 97(11), 2781-2791. DOI: 10.1002/cjce.23632.
- [32] Su, Z., Zhang, B., Cheng, X., Xu, M., Chen, G., Sha, Y., Wang, Y., Hu, J., Duan, R., Zhang, J. (2022). SnS₂/polypyrrole for high-efficiency photocatalytic oxidation of benzylamine. *Dalton Transactions*, 51, 13601. DOI: 10.1039/d2dt01899c.
- [33] Zhao, Y., Sun, D., Hu, K., Zhao, W., Huang, F. (2020). Surface defect engineering of SnS₂ nanocrystals for enhanced photocatalytic reduction of Cr(VI) under visible light, *Inorganic Chemistry Communications*, 114, 107849. DOI: 10.1016/j.inoche.2020.107849

- [34] Iqbal, M., Ibrar, A., Ali A., Hussain, S., Shad, S., Ullah, S., Alshahrani, T., Hakami, J., Khan, F., Thebo, K.H. (2022). Facile synthesis of Mn doped $\mathrm{Bi}_2\mathrm{S}_3$ photocatalyst for efficient degradation of organic dye under visible-light irradiation. Journal of Molecular Structure, 1267, 133598. DOI: 10.1016/j.molstruc.2022.133598.
- [35] Liang, P., Yuan, L., Du, K., Wang, L., Li, Z., Deng, H., Wang, X., Luo, S, Shi, W. (2021). Photocatalytic reduction of uranium (VI) under visible light with 2D/1D Ti₃C₂/CdS. Chemical Engineering Journal, 420, 129831. DOI: 10.1016/j.cej.2021.129831.
- [36] Du, P., Chang, J., Zhao, H., Liu, W., Dang, C., Tong, M., Ni, J., Zhang, B. (2018). Seabuckthorn-like MnO₂ decorated titanate nanotubes with oxidation property and photocatalytic activity for enhanced degradation of 178-estradiol under solar light. ACS Applied Energy Materials. 1(5), 2123-2133. DOI: 10.1021/acsaem.8b00197.
- [37] Qi, K., Liu, S., Qiu, M. (2018). Photocatalytic performance of TiO₂ nanocrystals with/without oxygen defects. *Chinese Journal of Catalysis*, 39, 867-875. DOI: 10.1016/s1872-2067(17)62999-1.